Received: 3 February 2023 | Revised: 15 May 2023 | Accepted: 1 June 2023

DOI: 10.1002/ese3.1505

REVIEW

Analysis of low-temperature pumped thermal energy storage systems based on a transcritical CO_2 charging process

Jonas Bodner[1] | **Josefine Koksharov**[1,2] | **Frank Dammel**[1,2] | **Peter Stephan**[1,2]

[1]Institute for Technical Thermodynamics, Technical University of Darmstadt, Darmstadt, Germany

[2]Darmstadt Graduate School of Excellence Energy Science and Engineering, Technical University of Darmstadt, Darmstadt, Germany

Correspondence
Josefine Koksharov, Institute for Technical Thermodynamics, Technical University of Darmstadt, Darmstadt, Germany.
Email: koksharov@ttd.tu-darmstadt.de

Abstract

Pumped thermal energy storage (PTES) is a technology for intermediate storage of electrical energy in the form of thermal energy. In this work, PTES systems based on a transcritical CO_2 charging process are investigated. A two-zone water storage tank with a storage temperature of 115°C is used as thermal energy storage. For discharge, an Organic Rankine Cycle (ORC) and, alternatively, a transcritical CO_2 heat engine are investigated. The considered concepts are modelled and simulated as stationary processes using the EBSILON *Professional* software. The scaling is based on an electrical input power of 5 MW. Using an ORC with the working fluid R1234yf for the discharging process results in the highest round-trip efficiency of 36.8%. The component costs of the different configurations are estimated using cost functions. On the basis of this, the levelized cost of storage (LCOS) is calculated. The configuration with the ORC as the discharging process has the lowest LCOS of 59.2 €cents $(kWh)^{-1}$. In addition, the technological maturity is determined using the technology readiness level scale. There are no prototypes of the investigated PTES systems yet. Therefore, further investigations must be carried out to implement the technology in the future.

KEYWORDS

CO_2 heat pump, energy storage, Organic Rankine Cycle, pumped thermal energy storage, transcritical CO_2

Abbreviations: CAES, compressed air energy storage; CEPCI, Chemical Engineering Plant Cost Index; CH, charging; CO_2, carbon dioxide; COP, coefficient of performance; DIS, discharging; G, generator; GWP, global warming potential; LCOE, levelized cost of electricity; LCOS, levelized cost of storage; M, motor; ODP, ozone depletion potential; ORC, Organic Rankine Cycle; PHS, pumped hydro storage; PTES, pumped thermal energy storage; RW, river water; ST, storage; TES, thermal energy storage; TRL, technology readiness level; TTD, terminal temperature difference; WG, water–glycol mixture.

1 | INTRODUCTION

Reducing greenhouse gas emissions is vital for slowing down climate change. Renewable energy sources such as solar and wind power are promoted but their fluctuation in power generation creates an imbalance in supply and demand. Thermal energy storage (TES) systems can help store energy on the timescales of these fluctuations. TES units are integrated into pumped thermal energy storage (PTES) systems, which operate through three subprocesses: charging, storage and discharging. Electrical energy is converted into thermal energy using an electrical heater or heat pump during the charging process. During discharge, a heat engine converts the thermal energy back into electrical energy using Rankine or Joule cycles.

There are many different variants of PTES systems. Zhao et al.[1] provide an overview of numerous studies in this regard. In this paper, different PTES concepts based on a transcritical CO_2 charging process are investigated. In such a Rankine cycle, the working fluid undergoes a supercritical change of state during heat transfer to the heat sink, here to the TES. In contrast to the subcritical change of state, the phase change between liquid and vapour takes place without the formation of a phase boundary. The supercritical change of state always exhibits a change in temperature. The course of the temperature can be adapted to that of a sensitive heat sink, and thus, the average temperature difference across the heat exchanger can be reduced. As a result, the efficiency of the process increases.[2]

There are already several publications on PTES systems with transcritical CO_2 cycles. In 2012, the first proposal of using CO_2 cycles in PTES systems along with ice slurry tanks as low-temperature TES was introduced by Mercangöz et al.[3] On the basis of this proposal, Morandin et al.[4,5] determined an optimal round-trip efficiency of 60% by using eight high-temperature TES and a maximum temperature in the discharging process of 177°C alongside ice slurry tanks as low-temperature TES with storage temperatures from −21.2°C to 0°C. It was found that the use of a throttle valve instead of an expansion machine in the charging process reduces the round-trip efficiency to 48%, while a complete expansion by means of an expander was suspected with technical problems due to the expansion in the two-phase region.

In 2013, Morandin et al.[6] focused on the thermoeconomic optimisation of the systems in the previous works with an electrical output power of 50 MW and charging durations of 2 h. The authors found that the efficiency at the lowest possible costs is optimised by superheating before compression in the charging process and using two independent high-temperature TES units. Pressure levels are directly related to the temperature differences in the heat exchangers, and optimisation should be carefully performed to achieve an optimal compromise between exergy losses in heat transfer and costs for heat exchangers. A round-trip efficiency of 64% was determined.

In contrast to the above-mentioned works, Baik et al.[7] considered in detail which pressure losses and heat transfer coefficients arise in the heat exchangers. They found that an optimal lower storage temperature exists for the high-temperature TES, which should not be too low, as the temperature profiles in the heat exchangers would separate from each other. The temperature should also not be too high as only a reduced part of the available heat could be used. Moreover, full utilisation of stored heat during the discharging process can lead to a reduced round-trip efficiency.

In the study of Steinmann et al.[8] conducted in 2020, a high-temperature TES system with a storage temperature of 160°C and an ice storage as low-temperature TES was investigated. The study found that the round-trip efficiency of this system was 45%, which is considered low compared with other PTES systems. The authors suggested that this PTES system may be better suited for combined provision of electricity, heating and cooling, and that a very large TES system would be required to achieve a higher round-trip efficiency. The study also found that the variation of the isentropic efficiencies of the compressor and the turbine had a minor influence on the round-trip efficiency.

Zhao et al.[9] investigated the use of sensible high-temperature TES with different storage fluids, including water, rapeseed oil and two synthetic heat transfer fluids. The study found that the use of an internal heat exchanger in both the charging and the discharging process increased the round-trip efficiency, energy density and specific purchase costs. The round-trip efficiency of this system was found to be 68%. The study highlights the importance of optimising the heat exchanger design to achieve an optimal compromise between exergy losses in heat transfer and costs for heat exchangers.

The majority of published works tend to neglect losses in motors and generators and rely solely on an expansion machine for the expansion during the charging process. As stated by Morandin et al.,[5] the latter could jeopardise technical feasibility. Therefore, this study considers losses in motors and generators, as well as a combination of both an expansion machine and a throttle valve. Although many studies have extensively investigated systems that use the same working fluid for charging and discharging, combinations of different working fluids, particularly with a transcritical CO_2 charging process, have not received enough attention. To address this research gap, this study explores also a configuration with an Organic Rankine Cycle (ORC) discharging process. It is important to note that different systems should not be evaluated solely based

on their round-trip efficiency, but also on their specific costs. Therefore, an economic analysis is conducted. Additionally, it is often unclear from published works to what extent the systems under consideration can be implemented, which is why the technology maturity is also examined in this study.

To achieve these goals, the main research objectives of the study presented here are:

- development of a numerical model and steady-state simulation of the considered PTES concepts; calculation of round-trip efficiency,
- estimation of the component costs and the levelized cost of storage (LCOS),
- determination of the technology maturity using the technology readiness level (TRL) scale of the European Commission.[10]

On the basis of these objectives, the concepts considered can be compared with each other or to other PTES systems. Thus, it can be decided which system represents the most promising variant for a future implementation and should consequently be part of further investigations.

2 | PTES SYSTEM CONCEPTS

In this section, the examined concepts are presented in detail. The structure of all subprocesses is shown schematically and the respective changes of state as well as their progressions in the *T*,*s*-diagram are outlined.

Currently, transcritical processes are mainly used in heat pumps with CO_2 as working fluid. The usage of CO_2 has some advantages: A supercritical temperature can be easily achieved, as the critical temperature is 31°C only. Due to a global warming potential (GWP) of 1 and an ozone depletion potential of 0, it has a low impact on the environment. Compared with other working fluids, CO_2 is inexpensive. Furthermore, it is neither flammable nor explosive, and it is only toxic above a volume fraction of 2%–3% in air. Therefore, CO_2 is used as the working fluid in the concepts considered in this work.[11]

A so-called two-zone storage system is used as a TES. This is a pressureless water storage tank with storage temperatures above 100°C. Such a storage temperature is possible by dividing the storage tank into two zones. Figure 1 shows the technology schematically. The water column of the upper zone above the lower one generates a pressure by its own weight, so that boiling water in the lower zone can be prevented without external pressurisation.[12]

In Germany, for example, such storage systems are already used for district heating and have a storage temperature of 115°C.[14] With specific costs of 400–700 € m^{-3}, the two-zone storage is the more cost-effective option compared with pressurised storage (800–1200 € m^{-3}).[15]

Two alternative discharging processes are investigated:

1. a subcritical ORC with different fluids,
2. a transcritical Rankine cycle with CO_2 as the working fluid.

These cycles are the favoured technology compared with other processes due to their more energy- and cost-efficient operation in generating electrical energy from

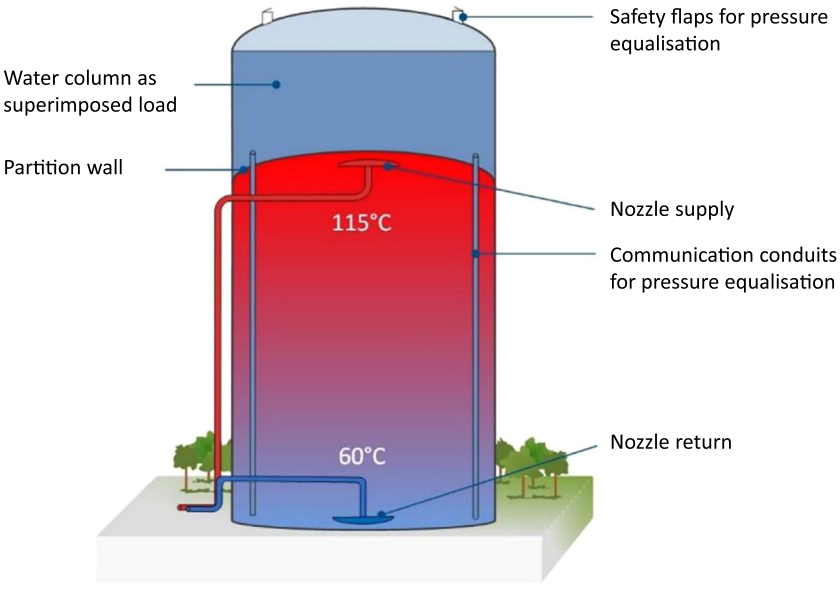

FIGURE 1 Two-zone storage.[13]

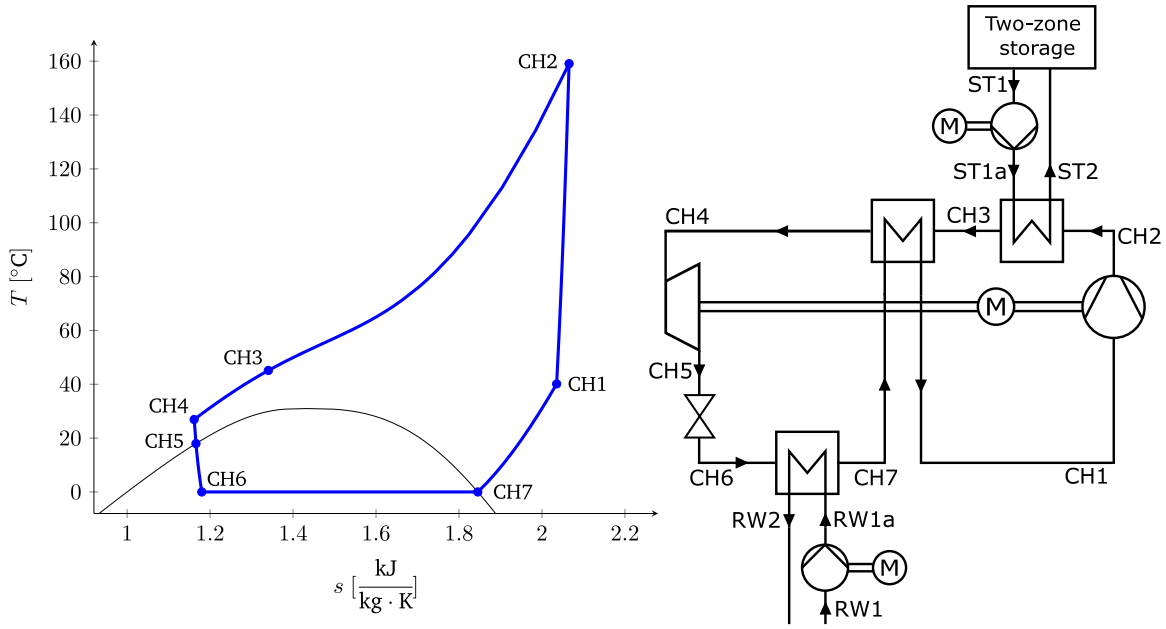

FIGURE 2 *T*,*s*-diagram (left) and schematic (right) of the CO_2 heat pump (configuration 1). CH, charging; M, motor; RW, river water; ST, storage.

low-temperature (<400°C) heat sources with limited capacity.[16]

In alternative 2, an ice storage is used as a heat source and sink in the charging and discharging process, respectively. This potentially increases the round-trip efficiency of the PTES system as the ice storage facilitates a more favourable temperature difference between hot and cold TES to be achieved. In addition, the location site independence is increased, since only the heat losses resulting from the irreversibility of the energy conversion have to be dissipated to the environment.[3]

2.1 | Configuration 1

2.1.1 | Charging process

The charging is carried out with the help of a transcritical CO_2 heat pump process as shown schematically in Figure 2 together with the corresponding *T*,*s*-diagram. Table 1 presents the changes of the state of the subprocess. The expansion is done by a combination of an expansion machine and a throttle valve. The working fluid is expanded from a supercritical pressure to saturation pressure in the expansion machine with the recovery of power. The remaining expansion in the two-phase region is carried out by the throttle valve. This ensures technical feasibility, as this approach has already been successfully tested by a manufacturer.[17] River water is used as a heat source. In addition, an internal heat exchanger is added to the circuit, as this achieves a significant improvement in the coefficient of performance (COP). This was verified by the steady-state simulation of the entire system.

TABLE 1 Changes of state for the CO_2 heat pump (configuration 1).

Change of state	Description
CH1–CH2	Compression to supercritical pressure
CH2–CH3	Heat rejection to the two-zone storage
CH3–CH4	Internal heat rejection
CH4–CH5	Expansion to just boiling liquid
CH5–CH6	Isenthalpic throttling into the two-phase area
CH6–CH7	Heat absorption with evaporation of the working fluid
CH7–CH1	Internal heat absorption

Abbreviation: CH, charging.

2.1.2 | Discharging process

The discharging process is conducted by means of an ORC. The configuration shown in Figure 3 is used. In addition, the associated *T*,*s*-diagram is depicted. The changes of state are listed in Table 2. The condensation of the working fluid takes place with heat dissipation to

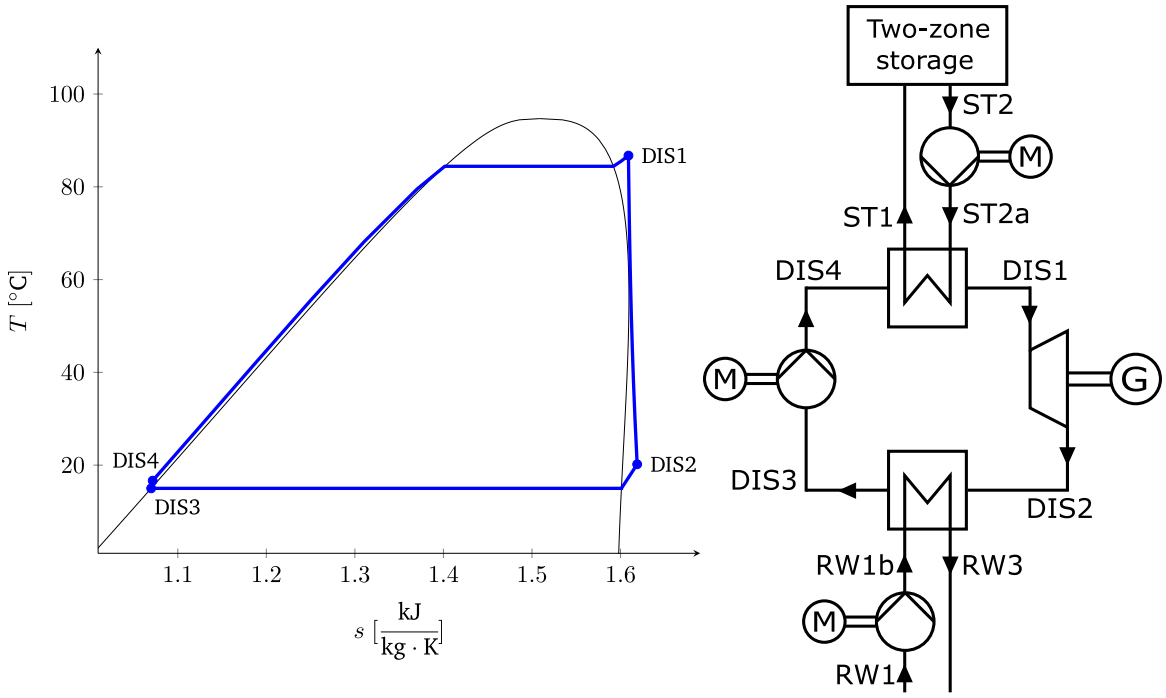

FIGURE 3 *T*,*s*-diagram (left) and schematic (right) of the ORC (configuration 1). DIS, discharging; G, generator; M, motor; ORC, Organic Rankine Cycle; RW, river water; ST, storage.

TABLE 2 Changes of state for the Organic Rankine Cycle heat engine (configuration 1).

Change of state	Description
DIS1–DIS2	Expansion of the vaporous working fluid
DIS2–DIS3	Heat rejection with condensation of the working fluid
DIS3–DIS4	Compression
DIS4–DIS1	Heating, evaporation and (if needed) superheating

Abbreviation: DIS, discharging.

river water. Initially, the working medium is not determined, which is why the use of different fluids is investigated. A detailed consideration of this is given in Section 3.1. An internal heat exchanger provides no relevant advantage, and therefore is not employed.

2.2 | Configuration 2

2.2.1 | Charging process

The charging process is the same as described in Section 2.1 for configuration 1 with the difference that an ice storage is used as the heat source during the evaporation of the CO_2. The related configuration scheme is shown in Figure 4. The changes of state are analogous to Section 2.1 except for the ice storage and the corresponding *T*,*s*-diagram also displays a similar shape. Since commercially available ice storage tanks cannot withstand the evaporation pressure of around 30 bar, the CO_2 cannot flow directly through the pipes of the ice storage tank, but an intermediate circuit is necessary.[18] For this purpose, a water–glycol mixture is used, which absorbs heat by freezing water in the ice storage and transfers it to the charging process.

2.2.2 | Discharging process

A heat engine with transcritical cycle and CO_2 as working medium is employed for discharging. Condensation takes place with heat dissipation to the intermediate circuit. For re-cooling, the heated water–glycol mixture flows through the ice storage, which in turn melts the ice. Since exergy is destroyed due to the irreversibility of the entire PTES system, more heat must be released in the discharging process than is absorbed in the charging process through the formation of ice. Two configurations, both fulfilling this requirement, are investigated:

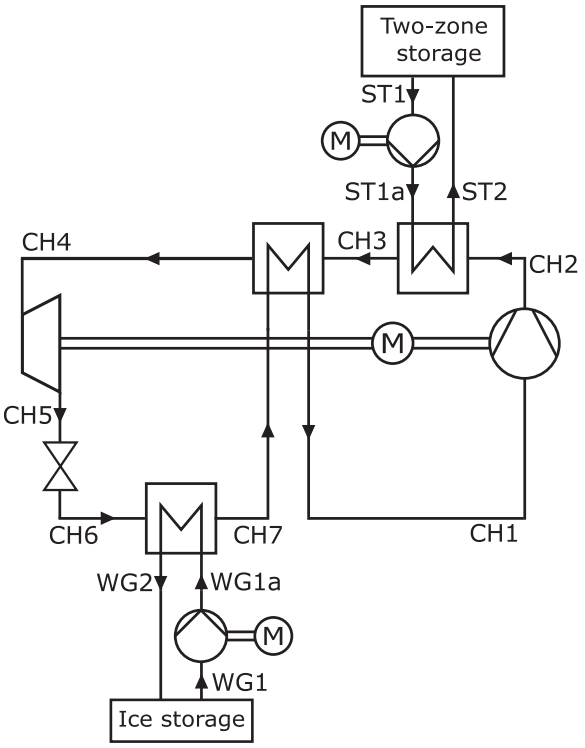

FIGURE 4 Schematic of the CO_2 heat pump (configurations 2a and b). CH, charging; M, motor; ST, storage; WG, water–glycol mixture.

(a) The environment is added as a heat sink: A river water cooling system is used to dissipate the excess heat.
(b) A share of the heat generated in the charging process is not fed into the discharging process, but utilised directly, for example, by integrating it into a district heating network. Thus, the ice storage represents the only heat sink in the discharging process.

Figure 5 shows the schematic and the *T*,*s*-diagram of configuration a. The changes of state are presented in Table 3. Configuration b, depicted in Figure 6, differs from this by the missing heat exchanger between the states DIS2 and DIS3 and the additional heat exchanger to extract heat to a district heating network. Both discharging processes do not experience any relevant advantage from an internal heat exchanger, which is why application is dispensed with.

3 | MODELLING AND SIMULATION

The modelling and the steady-state simulation of the PTES systems are carried out within the software EBSILON *Professional*. The modelling is done according to an object-based approach. Individual components of the real system are represented as objects and linked to each other according to the system structure. As a result, the model is very similar to circuit diagrams. The linking of the objects results in systems of equations which are solved numerically. Different working media are integrated via substance databases.[19]

In the modelling, all systems are scaled based on an input power of 5 MW and a charging and discharging time of 4 h each. The following assumptions are made for simplification:

- Specification of the isentropic, mechanical and electrical efficiencies of the components (see Table 4), and the assumption that these efficiencies are the same for all concepts.
- Neglect of heat losses in the subprocesses and during storage (a sharp boundary between areas of different temperatures in the TES is assumed): Due to this assumption and the constant charging durations, no implementation of the storage in the model is necessary for the stationary investigation.
- Neglect of pressure losses, since the information on the flow properties of the working fluid in the process required for the calculation is not available.
- River water temperature $T_{RW1} = 10°C$ and change of river water temperature by 5 K during heat exchange with the working fluid.
- Upper storage temperature in the two-zone storage tank $T_{ST2} = 115°C$; in analogy to the existing examples (cf. Section 2).
- Terminal temperature difference (for countercurrent heat exchangers, this corresponds to the temperature difference between the cold flow at its inlet and the warm flow at its outlet, or vice versa) in the heat exchangers ≥5 K: This way, the heat exchanger area required in each case is not too large and more scope is created for possible parameter fluctuations in reality. There are exceptions, which will be considered later in this section.
- Pinch temperature difference in the heat exchangers ≥0.1 K: This assures that the respective heat transfer is physically possible. Mostly, however, this is in the order of magnitude of the respective terminal temperature difference.

To enable a simulation of the systems, the initially variable parameters must be specified in addition to those defined in advance. Table 5 lists these and their constraints for the different configurations. To achieve the highest possible round-trip efficiency, the variable parameters are optimised in mutual dependence. This is

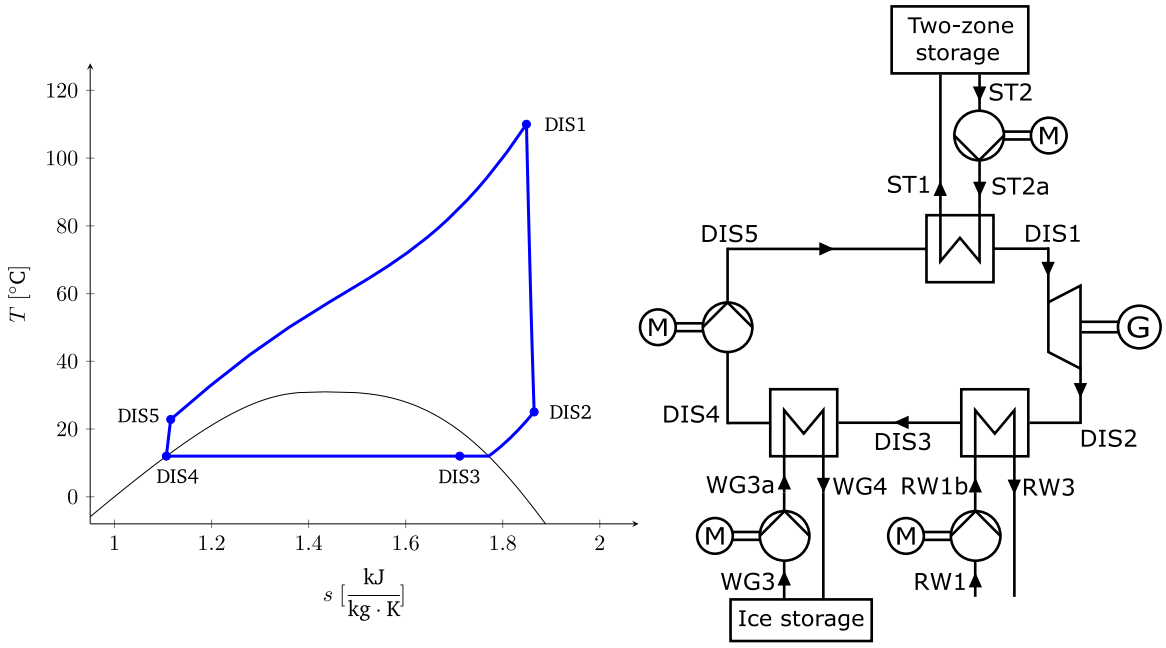

FIGURE 5 *T*,*s*-diagram (left) and schematic (right) of the CO_2 heat engine (configuration 2a). DIS, discharging; G, generator; M, motor; RW, river water; ST, storage; WG, water–glycol mixture.

TABLE 3 Changes of state for the CO_2 heat engine (configuration 2a).

Change of state	Description
DIS1–DIS2	Expansion
DIS2–DIS3	Heat rejection to river water
DIS3–DIS4	Heat rejection to the intermediate circuit with condensation of the CO_2
DIS4–DIS5	Compression to supercritical pressure
DIS5–DIS1	Heat absorption from the two-zone storage

Abbreviation: DIS, discharging.

done by means of a genetic algorithm using the optimisation tool EbsOptimize[20] integrated in EBSILON *Professional*.

The lower storage temperature T_{ST1} of the high-temperature TES in particular has a significant influence on the round-trip efficiency. While the COP of the charging process increases significantly with decreasing lower storage temperature T_{ST1}, the efficiency of the discharging process decreases substantially. Consequently, the optimal operating point corresponds to a compromise between the efficiencies of the subprocesses.

The variable parameters are chosen so that the terminal temperature differences in the heat exchangers are always as low as possible without violating the boundary condition (terminal temperature difference ≥5 K). Thus, the temperature profiles of working fluid and auxiliary fluid can be adapted to each other in the best possible way and consequently the efficiency of the heat transfer processes can be optimised. Since the required heat exchanger area increases with decreasing temperature difference, the costs for the required components also increase. With the help of an economic analysis (see Section 4), it is individually evaluated whether the additional financial expenditure is justified. Due to the specification of a minimum terminal temperature difference of 5 K, the optimisation does not result in disproportionately large heat exchanger areas, which is why the results also make sense from an economic point of view.

In the following, some individual characteristics of the different concepts are considered.

3.1 | Configuration 1

To avoid damage to the turbine blades by liquid, a steam content of $x = 1$ during the entire expansion process in the turbine of the ORC is set as a constraint for the optimisation. Complete evaporation in state DIS1 is therefore essential. If the working fluid is a wet fluid (thus, the slope of its saturation vapour curve in the *T*,*s*-diagram is negative), additional superheating is mandatory. Furthermore, for dry fluids (the slope of their saturation vapour curve is positive), superheating is necessary if the evaporation temperature is greater than the temperature at which the saturation vapour

curve has the greatest gradient ($dT/ds \to \infty$) in the T, s-diagram. If superheating does not occur in this case, the two-phase region is passed through during expansion.

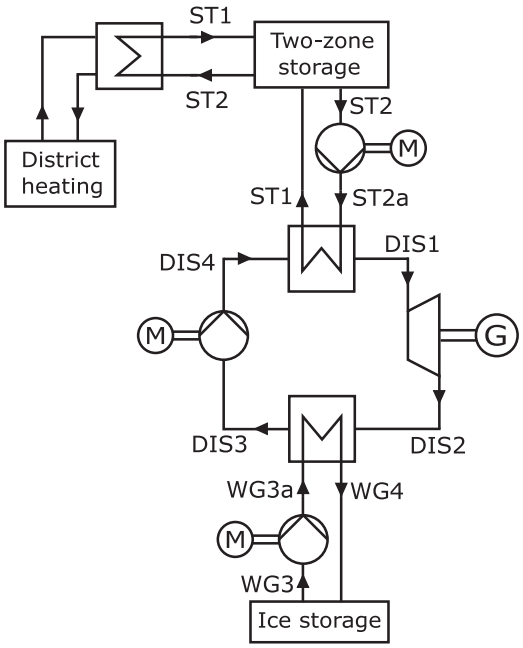

FIGURE 6 Schematic of the CO_2 heat engine (configuration 2b). DIS, discharging; G, generator; M, motor; ST, storage; WG, water–glycol mixture.

TABLE 4 Component efficiencies.

Component	Parameter	Value	Parameter	Value
Compressor	$\eta_{is,Com}$	0.85	$\eta_{mech,Com}$	0.99
Liquid expander	$\eta_{is,Exp}$	0.85	$\eta_{mech,Exp}$	0.99
Pump	$\eta_{is,P}$	0.80	$\eta_{mech,P}$	0.99
Turbine	$\eta_{is,T}$	0.90	$\eta_{mech,T}$	0.99
Motor	$\eta_{el,M}$	0.95	$\eta_{mech,M}$	0.99
Generator	η_G	0.98		

Abbreviations: Com, compressor; Exp, expansion machine; G, generator; is, isentropic; M, motor; mech, mechanical; P, pump; T, turbine.

To limit the selection of potential working fluids for the ORC, a preselection is made using the REFPROP database.[21] Thereby, the available fluids are filtered according to the following criteria:

1. It is a fluid from the common fluids category in REFPROP: This selection is made to ensure market availability and to ensure it is not a completely new and unexplored fluid.
2. The substance has a critical temperature of at least 340 K (66.85°C): Since the evaporation temperature in the discharging process is below the critical temperature, the critical temperature should be large enough so that the most efficient use of the heat provided by the TES can be realised. This is achieved by a low-temperature difference during heat transfer, which in turn is achieved by a sufficiently high temperature of the working fluid.
3. The fluid has a boiling temperature (at a pressure of 1 bar) of at most 300 K (26.85°C): To achieve a high efficiency, the condensation pressure p_{DIS2} should be as low as possible, but not less than 1 bar, so that infiltration of the working fluid by entering air is avoided in the case of leakage.[22–24] If the boiling temperature of the working fluid at 1 bar is greater than 300 K, this results in an increased average temperature of the working medium when it gives off heat to the cooling water. This leads to a lower efficiency.

As a further criterion, a GWP of less than 150 is determined according to European Union regulation 517/2014.[25] The following eight fluids meet all conditions and are considered as potential working fluids: ammonia, butane, isobutane, propane, propene, R1234yf, R1234ze (E) and R152a.

3.2 | Configuration 2

For the intermediate circuit that connects the charging or discharging process with the ice storage, a water–glycol mixture with a glycol content of 30 vol% is used.

TABLE 5 Optimised parameters and their constraints.

Configuration	1	2a	2b
Optimised parameters	T_{ST1}, T_{CH1}, p_{CH2}, T_{CH3}, p_{CH6}, T_{DIS1}, p_{DIS2}, T_{DIS3}, p_{DIS4}	T_{ST1}, T_{CH1}, p_{CH2}, T_{CH3}, p_{CH6}, T_{DIS1}, p_{DIS2}, T_{DIS4}, p_{DIS5}	T_{CH1}, p_{CH2}, T_{CH3}, p_{CH6}, T_{DIS1}, p_{DIS2}, T_{DIS3}, p_{DIS4}
Constraints	$TTD \geq 5$ K, $x_{DIS1DIS2} = 1$	$TTD \geq 5$ K, TTD (heat transfer processes at the respective lower pressure level) ≥ 2 K	$TTD \geq 5$ K, TTD (heat transfer processes at the respective lower pressure level) ≥ 2 K

Abbreviations: CH, charging; DIS, discharging; ST, storage; TTD, terminal temperature difference.

The implementation of an ice storage potentially increases the round-trip efficiency of the PTES system, as the condensation temperature in the discharging process can be reduced and thus the efficiency of the subprocess can be increased. In order that the heat released from the ice storage during the charging process can be reabsorbed during the discharging process, it is necessary that the evaporation temperature T_{CH6} of the CO_2 in the charging process is lower than the condensation temperature T_{DIS3} in the discharging process. Since a temperature difference is required for all heat transfer processes between the water–glycol mixture and the CO_2 or the ice storage, there is a certain minimum temperature difference ΔT required between the above-mentioned temperatures T_{CH6} and T_{DIS3}, which results from the sum of the temperature differences of the individual heat transfer processes. If the minimum terminal temperature difference is set at 5 K, as explained before, ΔT becomes so large that the efficiency advantage due to the ice storage disappears. As a result, the minimum terminal temperature difference is reduced to 2 K for all heat transfer processes that take place at the respective lower pressure level. As a consequence, the required heat exchanger area and therefore the purchase costs of the components increase.

Furthermore, another boundary condition is specified for configuration b (direct use of a share of the stored energy in the two-zone storage tank) since the lower storage temperature T_{ST1} in the TES must be higher than the return temperature of the district heating network in the case of integration into one. The optimal temperature T_{ST1} in terms of maximum electricity yield is around 25°C and the efficiency decreases with increasing temperature T_{ST1}. Therefore, the assumption of a return temperature of around 60°C, as is currently common in many district heating networks, is not reasonable.

However, as part of the future further development of district heating networks, the lowering of distribution temperatures is considered a decisive factor in the decarbonisation of district heating. Return temperatures could be reduced to around 30°C, which is why this temperature is used as a reference point in this work. Thus, the lower storage temperature for configuration b is assumed to be $T_{ST1} = 35$°C.[26]

3.3 | Results

Table 6 gives an overview of the simulation results for the different configurations. The energy density is calculated from the ratio of energy released in a discharge cycle to the total storage volume, which is composed of the respective volumes of the two-zone storage and the ice storage. R1234yf proves to be the best working medium for the ORC in configuration 1. In this configuration, it is also investigated how the system behaves if only the throttle valve is used for the expansion in the charging process. In this case, a reduced round-trip efficiency of 33.8% results. However, the purchase costs would be lower, as no expansion machine would be needed in the charging process. Considering the LCOS, it is examined in Section 4.2 whether the reduced financial expenditure is justified to the detriment of efficiency.

TABLE 6 Simulation/optimisation results.

Configuration	1	2a	2b
Charging process			
Fluid	CO_2	CO_2	CO_2
COP	3.07	3.13	2.92
$\eta_{ex,CH}$ (%)	58.0	54.4	53.4
Storage			
Storage temperature in the two-zone storage	40.1–115°C	28.4–115°C	35–115°C
Decoupled heat (MW)	None	None	3.21
Discharging process			
Fluid	R1234yf	CO_2	CO2
$\eta_{th,DIS}$ (%)	12.0	10.7	11.6
$\eta_{ex,DIS}$ (%)	63.5	61.7	63.7
Energy density (kWh m^{-3})	5.43	3.85	3.96[a]
η_{rt}	36.8	33.6	33.8[a]

Abbreviations: CH, charging; COP, coefficient of performance; DIS, discharging; ex, exergetic; rt, round-trip; th, thermal.

[a]Both energy density and round-trip efficiency are calculated taking into account the exergy of the decoupled heat flow. It is assumed that the district heating water is heated to 65°C while the return temperature is 30°C.

Configuration 1 has both the highest round-trip efficiency and the highest energy density, measuring 36.8% and 5.43 kWh m^{-3}, respectively. The higher energy density is due to the fact that, unlike the other two configurations, no ice storage is required.

In configuration 2b, a heat flow of 3.21 MW is decoupled in addition to the output power of 1.32 MW. Due to the increased lower storage temperature $T_{ST1} = 35$°C, the COP of the charging process is lower compared with configuration 2a ($T_{ST1} = 28.4$°C). However, since no heat must be released to the environment in the discharging process, the condensation temperature T_{DIS3} can be reduced, which is why the efficiency of the discharging process is higher than in configuration 2a.

4 | ECONOMIC ANALYSIS

In this section, the purchase costs of the components and the LCOS of the considered concepts are calculated. In addition, a sensitivity analysis is carried out regarding the LCOS.

4.1 | Component costs

The procedure according to Turton et al.[27] is used to estimate the purchase costs of most components. Here, the costs of a component are calculated from predefined factors and a characteristic value of the component, such as its power or dimensions. The characteristic values are taken from the simulated model.

The characteristic size of a heat exchanger is its area. The simulation results, on the other hand, provide the product of heat exchanger area and overall heat transfer coefficient U. To enable the calculation of the areas, the respective overall heat transfer coefficients are estimated using literature values. Some of the values are not determined directly from the literature, but from the respective heat transfer coefficient h.

Since very large heat transfer coefficients occur during phase change and the thermal resistance of the wall between the fluids is usually low, both values are neglected in the calculation. Consequently, the overall heat transfer coefficient U with one-sided phase change corresponds to the heat transfer coefficient h of the fluid without phase change. If the heat transfer coefficient on both sides is taken into account, the overall heat transfer coefficient results according to $U = (h_1^{-1} + h_2^{-1})^{-1}$. Table 7 provides an overview of the values used.[28]

To verify the results according to Turton et al.[27] and to estimate the costs of the pump in the CO_2 discharging process, the cost functions according to Morandin et al.[6] are employed.

The estimation of the costs of generators is based on the simple relationship also known as the six-tenths rule.[27] The data of the reference generators are taken from the publication by Balli et al.[36]

The estimation of the costs of the two-zone storage is done with the help of the specific costs given by Maximini.[15] The mean value $C_{spec} = 550\,€\,m^{-3}$ is used for the calculation. It is assumed that the TES is fully loaded after each charging cycle and fully unloaded after each discharging cycle.

The costs of the ice storage are calculated using the cost function according to Sanaye and Shirazi.[37] A complete loading or unloading is also assumed.

The data for calculating the various components come from different years. To take price fluctuations and inflation into account, all component costs are related to the same reference year with the help of a cost index, the Chemical Engineering Plant Cost Index (CEPCI). Since

TABLE 7 Convective and overall heat transfer coefficients.

Fluid		h (W [m² K]$^{-1}$)		Sources
Water (liquid)		1000		[28]
CO_2 (supercritical, cooled)		2000		[29, 30]
CO_2 (supercritical, heated)		2000		[31]
CO_2 (near critical temperature)		3000		[29, 30]
CO_2 (vapour)		500		[32]
Water–glycol mixture		700		[33]
Hot fluid	**Cold fluid**	**Phase change**	**U (W [m² K]$^{-1}$)**	**Sources**
Water	CO_2	Evaporation	1000	[28]
CO_2 (near critical temperature)	CO_2 (vapour)	–	429	[29, 30, 32]
CO_2 (supercritical)	Water	Supercritical condensation	667	[28–30]
Water	R1234yf	Evaporation	500	[28, 34]
R1234yf	Water	Condensation	700	[34, 35]
Water	CO_2 (supercritical)	Supercritical evaporation	667	[28, 31]
CO_2 (vapour)	Water	–	333	[28, 32]
Water–glycol mixture	CO_2	Evaporation	700	[33]
CO_2	Water–glycol mixture	Condensation	700	[33]

TABLE 8 Total component costs of the configurations.

Configuration	Total component costs (10^6 €)
1	4.23
2a (for dual use of components)	5.51 (4.94)
2b (for dual use of components)	4.88 (4.30)

average CEPCI values for recent years are not freely available at the time of this work, 2019 is chosen as the reference year.[38] For conversion into euros, the official exchange rate of the European Commission[39] is used.

Since configurations 2a and b use the same working fluid in both the charging and discharging processes, it is possible to use some of the components in both subprocesses. This concerns the heat exchangers to the energy storage tanks and the pumps that pump the water or the water–glycol mixture through these heat exchangers. Thus, the total component costs of the configurations are reduced.

Table 8 gives an overview of the total component costs of the different configurations. Configuration 1 has the lowest component costs at 4,232,000 €. Even with the dual use of some components, the other configurations have higher purchase costs. This is mainly due to the increased costs for the heat exchangers resulting from the reduced temperature differences within the heat exchangers. The temperature difference in the heat transfer from the hot TES to the discharging process, for example, is low because the temperature curves are well matched due to the supercritical change of state. In addition, the minimum terminal temperature difference in some heat exchangers is reduced, which is why the required heat exchanger areas also increase. Furthermore, a more powerful pump is needed in the discharging process to realise the compression to the supercritical pressure.

Figure 7 compares the shares of the costs of the different components for configurations 1 and 2a. The three subprocesses charging, storage and discharging are shown in different colours. The compressor, including the corresponding motor, is the most cost-intensive component.

4.2 | Levelized cost of storage

The LCOS is the specific cost of discharging one unit of electrical energy. It represents the equivalent quantity to the levelized cost of electricity (LCOE) for electricity generation technologies. The result is subject to uncertainties since the development of all parameters must be forecast over the entire lifetime of the respective plant. The LCOS results from the ratio of the economic expenditure of a plant over its lifetime and the total amount of electricity discharged. The costs incurred through compound interest are also considered. Assuming that the annual operating costs and the amount of electricity discharged per year are constant over the lifetime of the PTES system, the LCOS is calculated according to the following equation.[40,41]

$$LCOS = \frac{I + C_{\mathrm{op}} \cdot \sum_{t=1}^{n} \frac{1}{(1+i)^t}}{E_{\mathrm{el}} \cdot \sum_{t=1}^{n} \frac{1}{(1+i)^t}} + \frac{c_{\mathrm{el,in}}}{\eta_{\mathrm{rt}}}.$$

In Steinmann et al.,[42] a running time between 20 and 30 years is expected for PTES systems. Therefore, the running time of the system is assumed to be $n = 25$ years in this study. A charging and discharging time of 4–6.5 h is discussed in Krüger et al.[43] as potential economic and operational viability. Here, the lower limit of 4 h is assumed and one charging and one discharging cycle are to be carried out 365 days a year. Consequently, the amount of electrical energy released per year is calculated as $E_{\mathrm{el}} = 365 * 4\,\mathrm{h} * P_{\mathrm{out}}$.

In addition to the component costs, the investment costs also consist of further costs for, for example, pipelines, measuring devices, buildings and personnel.[44] To determine the investment costs I from the sum of the purchase costs of all components C_{c}, the so-called Lang factor, in this case $F_{\mathrm{lang}} = 4.74$, is utilised. Consequently, the investment costs are calculated with $I = F_{\mathrm{lang}} * C_{\mathrm{c}}$.[27]

To estimate the annual operating costs C_{op}, the factor $F_{\mathrm{op}} = 0.015$ is introduced. The operating costs include all costs for operating personnel, maintenance work, administration and materials for maintenance. The calculation is made by multiplying the factor F_{op} by the total investment costs of the plant.[45]

$c_{\mathrm{el,in}}$ is the specific purchase cost of the electrical energy supplied. Dietrich[46] derived a characteristic operating scenario from the day-ahead market for electricity, which has good predictability due to daily repeatability. The hourly average prices determined over a year show a global minimum in the early morning hours and a global maximum in the evening hours. It is assumed that the purchase is made in the cheapest 4-h block per day in the early morning hours. Applying the method of Dietrich[46] to the year 2019 using the values from ENTSO-E,[47] the purchase costs are assumed to be $c_{\mathrm{el,in}} = 2.576$ €cents $(\mathrm{kWh})^{-1}$.

The coefficient i is the real imputed interest rate. In this work a debt capital share of 100% is assumed, which is why only the interest rate of the debt capital is considered.

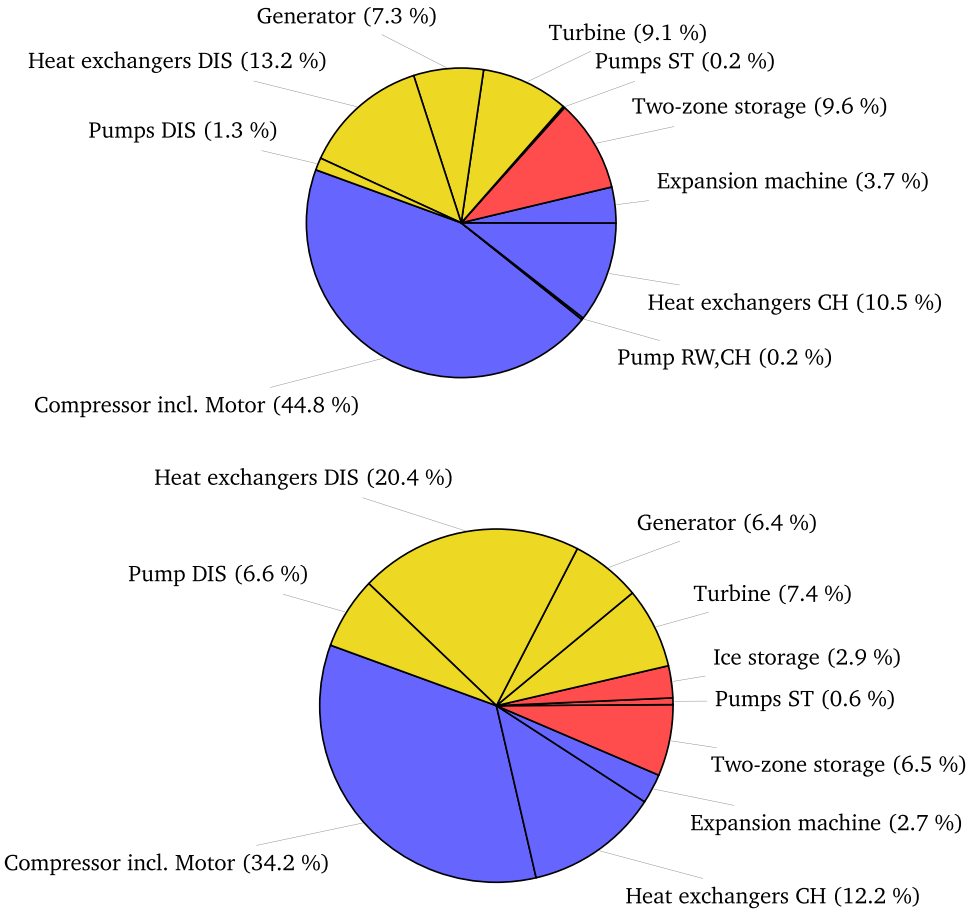

FIGURE 7 Shares of the costs of the different components for configurations 1 (top) and 2a (bottom). The difference in the size of the areas is scaled according to the difference in cost. Blue, charging (CH); red, storage (ST); yellow, discharging (DIS). RW, river water.

The effective interest rate of the KfW bank's promotional programme "Erneuerbare Energien Standard" (engl.: Renewable Energies Standard) is used as the interest rate on debt capital. This is a programme for the low-interest financing of any renewable energy system.[48]

Within the scope of this work, financing at an effective interest rate of $i_{\text{eff}} = 3.81\%$ with a fixed interest rate of 20 years is assumed.[49]

Since the running time of the PTES system under consideration is 25 years, it is assumed that the same interest rate applies for a fixed interest rate of 25 years. To determine the real imputed interest rate from the selected effective interest rate, which is a nominal value, it is necessary to take the inflation rate into account. Analogous to the study of the Fraunhofer institute[40] regarding the LCOE of renewable energies, an annual inflation rate of $i_{\text{inflation}} = 1.2\%$ is assumed.

The real imputed interest rate i is calculated according to $i = i_{\text{eff}} - i_{\text{inflation}}$, known as the Fisher equation.[50]

Table 9 shows the results of the calculation of the LCOS. The LCOS of configuration 2b is not directly comparable with the other values, as the additional heat generated is not taken into account.

As configuration 1 has the highest round-trip efficiency and the lowest component costs, it has the lowest LCOS. Relatively, the LCOS of configuration 2a is over 38% higher. With dual use of some components, the LCOS is also significantly higher (by more than 25%). From an economic point of view, configuration 1 should therefore be the subject of further development.

If the expansion machine in the charging process is omitted in configuration 1, that is, expansion takes place in the throttle valve alone, the LCOS is slightly higher, although the component costs are lower. This is due to the lower round-trip efficiency. Consequently, this change to the configuration should be rejected.

4.3 | Sensitivity analysis of the LCOS

To estimate the influence of the different coefficients on the LCOS and thus the effect of inaccuracies, a sensitivity analysis is carried out. The varied parameters and the results

of the sensitivity analysis for configuration 1 are shown in Table 10. The given interval of the investment costs results from the average deviation of the component costs.[27] The upper and lower values for electricity purchase costs are derived from day-ahead market values[47] for 2017 and 2021, respectively. To investigate the influence of the charging and discharging time on the LCOS, an interval between 3 and 5 h was selected. Only one configuration is examined, as the results of all configurations are analogous. There would only be differences in the absolute values. The variation of the investment costs has the greatest influence on the result with a relative deviation of approximately ±29%. The charging and discharging duration also has a major influence, as shown by a deviation of 26% for a duration of 3 h. In this study, the electricity purchase costs refer to the year 2019. The result of the sensitivity analysis shows that the purchase costs have less influence on the LCOS in earlier years. However, the purchase costs increased significantly during the year 2021, affecting the LCOS by 19%. With deviations of up to 12% and 10%, the running time and the interest rate also have a significant influence on the result. Due to the great uncertainty in the estimation and possibly the following large deviations, the determined value for the LCOS should not be used to assess the economic efficiency of a plant. However, it can be used to compare different concepts and as a basis for deciding whether a modification of a configuration is reasonable from an economic point of view. When actually determining the economic viability of the plant, the parameters should be chosen as accurately as possible to obtain a reliable result.

TABLE 9 LCOS of the configurations.

Configuration	LCOS (€cents [kWh]$^{-1}$)
1 (only throttle valve in the charging process)	59.2 (59.8)
2a (for dual use of components)	82.3 (74.5)
2b[a] (for dual use of components)[a]	91.9 (81.9)

Abbreviation: LCOS, levelized cost of storage.

[a]In the calculation, the $c_{el,in}/\eta_{rt}$ term only considers the share of the supplied electricity that is not used to generate the decoupled heat.

5 | TECHNOLOGY READINESS LEVEL

The technology maturity of the concepts is determined based on the TRL scale of the European Commission.[10] The TRL scale comprises nine levels, whereby the technology maturity increases with the increasing level number. Table 11 depicts the levels and their respective requirements.

First, the TRLs of the subprocesses are determined, followed by the TRLs of the overall concepts.

5.1 | Evaluation of the subprocesses

5.1.1 | CO_2 heat pump

Several CO_2 heat pumps in the smaller capacity range (up to 1.2 MW heating capacity) are already in use.

TABLE 10 Sensitivity analysis of the LCOS for configuration 1.

Parameter	Value	Variation of the LCOS (%)
Investment costs I	13.54 • 10^6 €	−29
(Base case: 20.06 • 10^6 €)	26.58 • 10^6 €	+29
Factor for operating costs F_{op}	1%	−6
(Base case: 1.5%)	2%	+6
Running time of the plant n	20 years	+12
(Base case: 25 years)	30 years	−8
Effective interest rate i_{eff}	2.69%[49]	−9
(Base case: 3.81%)	5.05%[49]	+10
Electricity purchase costs $c_{el,in}$	2.233 €cents (kWh)$^{-1}$	−2
(Base case: 2.576 €cents [kWh]$^{-1}$)	6.640 €cents (kWh)$^{-1}$	+19
Charging and discharging duration	3 h	+26
(Base case: 4 h)	5 h	−16

Abbreviation: LCOS, levelized cost of storage.

TABLE 11 TRL scale according toDe Rose et al.[10]

Phase	TRL	Requirement
Research	1	Basic principles observed
	2	Technology concept formulated
	3	Experimental proof of concept
Development	4	Technology validated in lab
	5	Technology validated in relevant environment
	6	Technology pilot demonstrated in relevant environment
Deployment	7	System prototype demonstration in operational environment
	8	System complete and qualified
	9	Actual system proven in operational environment

Abbreviation: TRL, technology readiness level.

However, the entire expansion takes place by means of a throttle valve.[51]

A configuration such as that contained in the concepts considered here has been successfully tested on a test rig by MAN Energy Solutions. The company also offers all the necessary components.[52]

Consequently, the subprocess is assessed with TRL6. TRL7 is not achieved as there is no evidence that the function of a large-scale prototype has been demonstrated in its operational environment. As the MAN Energy Solutions' heat pump is expected to be deployed as early as April 2023, further development to TRL8 is expected by then.[53,54]

5.1.2 | Two-zone storage tank

Four examples of the two-zone storage tank are already in use in Germany, which is why the technology is rated TRL8.[14] To reach TRL9, there would have to be widespread distribution in the market.

5.1.3 | Ice storage

Ice storage systems are commercially widespread and various companies offer them.[55–57] Consequently, the system is rated TRL9.

5.1.4 | ORC with R1234yf as working fluid

Numerous ORC systems are in use worldwide. However, the working fluid R1234yf has never been used so far in ORC processes. TRL3 is achieved because the technology concept has been investigated, formulated and verified by numerical simulation.[58] TRL4 is not achieved because there is no prototype or experimental investigations yet.

5.1.5 | CO_2 heat engine

Transcritical CO_2 heat engines have been investigated several times on an experimental level.[11] One manufacturer already provides such a system commercially, but with a much higher temperature of the heat supply. While this temperature is 532°C in the standard case, the heat supply in the context of this work takes place at a temperature of 115°C.[59]

TRL6 is not achieved as the system has not been tested under the operating conditions in this work. Consequently, the CO_2 discharging process is assessed as TRL5.

5.2 | Evaluation of the complete systems

5.2.1 | Configuration 1

All subsystems of this configuration have at least TRL3. In addition, integration into the overall system is expected to be straightforward. The feasibility is demonstrated in this work by means of the numerical model and crucial parameters are identified. Consequently, the maturity of the technology is assessed according to TRL3.

5.2.2 | Configuration 2 (a and b)

Configurations 2a and 2b are assessed together, as the differences do not affect the TRL evaluation. All subsystems have at least TRL5 and the model of the complete system was analysed numerically as part of this work. The configurations do not reach TRL4, as no information is available regarding a prototype or experimental investigations of the overall systems. Accordingly, the classification is TRL3. However, since all subsystems already have at least TRL5, comparatively rapid development could be possible in the future.

6 | DISCUSSION OF THE RESULTS

Due to the progression of the supercritical change of state in the CO_2 heat engine (configuration 2), a temperature of $T_{DIS1} = 110$°C can be reached at the

inlet of the turbine. For the ORC (configuration 1), this temperature is $T_{DIS1} = 87.6°C$. Although this enables 500 kW more power to be generated by expansion in the turbine in configuration 2a than in configuration 1, the latter has a higher round-trip efficiency. On the one hand, this is due to the high power demand of the pump, which is caused by the required pressure increase of more than 90 bar. On the other hand, the efficiency-increasing potential of the ice storage by lowering the temperature at the outlet of the turbine T_{DIS2} cannot be exploited well with the CO_2 heat engine. In configuration 2a, some heat must be dissipated to the environment, which is why its temperature limits a potential reduction of T_{DIS2}. In configuration 2b, the temperature is limited by the required temperature differences in the heat transfer processes between the ice storage and the charging or discharging process, as described in Section 3.2. In addition, the round-trip efficiency is reduced by setting the lower storage temperature of the two-zone storage to $T_{ST1} = 35°C$.

The PTES systems with CO_2 cycles from the publications considered in Section 1 have significantly higher round-trip efficiencies. This is mainly the case because other TES systems are used.

On the one hand, the low-temperature TES are either integrated as ice storage without an intermediate circuit or as ice slurry storage tanks. In both variants, there is a direct heat transfer between the storage tank and the subprocess, which is why the temperature difference between the evaporation temperature T_{CH6} during charging and the condensation temperature T_{DIS3} during discharge can be selected lower. The disadvantage of ice slurry systems is that they have higher initial costs than ice storages and are less common.[60] Therefore, a lower TRL is to be expected. The implementation of an ice storage without an intermediate circuit is not possible because the pressure of the working fluid CO_2 is too high.[18]

On the other hand, pressurised water storage tanks with significantly higher storage temperatures than assumed in this work are used in the publications as high-temperature TES.[4,6,8] In addition, several high-temperature storage units are used there, and the mass flow of the storage medium is adjusted in such a way that the temperature difference to the working fluid CO_2 is kept as low as possible. This requires several heat exchangers and significantly increases the complexity of the system. These modifications contribute to higher round-trip efficiency.

Furthermore, in contrast to this work, most publications neglect losses in the motors and generators and the expansion in the charging process is carried out exclusively by means of an expansion machine. As explained in Sections 2.1 and 5, the latter could jeopardise technical feasibility.

Several publications analyse the potential of PTES systems in terms of round-trip efficiency depending on the selected storage and ambient temperature. On the basis of the formula developed by Thess,[61] which was later corrected by Chen and Guo,[62] a limit of $\eta_{rt} = 40.15\%$ results for the present configurations. According to the analysis by Roskosch et al.,[63] which attempts to use realistic simple Rankine cycles as a basis, a limit of approximately $\eta_{rt} = 47\%$ emerges. The round-trip efficiencies in this study are relatively close to these values, hence it is assumed that the configurations presented are reasonable for the selected storage and ambient temperature.

In this work, simplifications such as the neglect of storage, heat and pressure losses are assumed for all configurations, which would lead to significant efficiency losses in reality. Consequently, lower round-trip efficiencies are to be expected.

The energy density of the presented systems is low compared with other PTES systems. The review by Vecchi et al.[64] shows other studies reaching values of up to 110 kWh m^{-3}. The energy densities achieved here are relatively low because, on the one hand, there are no large temperature differences in the hot TES and, on the other hand, the efficiencies of the discharge processes are low. Therefore, a large volume of storage medium, in this case water, is required to discharge a certain amount of energy.

Compared with the established energy storage technologies, compressed air energy storage (CAES) and, in particular, pumped hydro storage (PHS), the PTES configurations of this study are characterised by a smaller installation footprint and no requirement for specific geographical constraints that significantly limit their use. CAES and PHS, on the other hand, have a much higher round-trip efficiency with values of over 70%. In addition, their technology maturity is higher, as these storage systems are already in commercial use. The energy density of the configurations presented is more than twice that of PHS systems, while CAES systems achieve similar energy densities.[65]

The determination of the economic key figures of the configurations is carried out under considerable uncertainties. For example, the cost functions of Turton et al.[27] have an accuracy in the range of +40 to −25%. The results of the sensitivity analysis of the LCOS (Table 10) show the impact that inaccuracies can have.

7 | SUMMARY AND CONCLUSION

In this work, PTES systems based on a transcritical CO_2 charging process were numerically modelled and simulated stationary with the software EBSILON

Professional. The scaling is based on the specification of a supplied electrical power of 5 MW. A so-called two-zone storage tank is used as a high-temperature TES. For discharge, an ORC with an initially undefined working medium and a transcritical CO_2 process are investigated. When using the latter process, an ice storage is also implemented.

Configuration 1 (ORC as a discharging process) has the highest round-trip efficiency with a value of 36.8% when using R1234yf as the working fluid of the discharging process.

The component costs of the different configurations are estimated using cost functions. With a share of more than 30% of the total component costs, the compressor including the associated motor is the most cost-intensive component in all configurations.

The LCOS is calculated based on the component costs. With LCOS of 59.2 €cents $(kWh)^{-1}$, configuration 1 is the most cost-effective. The examined configurations with the CO_2 discharging process have LCOS of at least 74.5 €cents $(kWh)^{-1}$ and are thus considerably more cost-intensive.

Furthermore, the technology maturity of the sub-processes and the overall systems is determined using the TRL scale. Since no prototypes of the PTES systems under consideration exist yet, their technology maturity is classified as TRL3. Consequently, some development is still needed before actual implementation.

Due to the highest round-trip efficiency and the lowest LCOS, configuration 1 is the most promising variant. Consequently, this system should be the subject of future investigations. In particular, the effect of the simplifications made, the impact of ambient temperature deviation and the transient behaviour could be examined to obtain more detailed information about the efficiency of the system.

NOMENCLATURE

c	specific costs (€cents $(kWh)^{-1}$)
C	costs (€)
E	produced energy per year (kWh)
F	factor (–)
h	(convective) heat transfer coefficient $(W\,(m^2\,K)^{-1})$
i	interest rate (–)
I	investment costs (€)
n	running time (a)
p	pressure (bar)
P	power (W)
$\dot{Q}$	heat flow (W)
s	specific entropy $(J\,(kg\,K)^{-1})$
t	time (h)
T	temperature (°C)
U	overall heat transfer coefficient $(W\,(m^2\,K)^{-1})$
x	steam content (–)

GREEK SYMBOLS

Δ	difference (–)
η	efficiency (–)

SUBSCRIPTS

c	component
CH	charging
Com	compressor
DIS	discharging
eff	effective
el	electrical
ex	exergetic
Exp	expansion machine
G	generator
in	input
is	isentropic
M	motor
mech	mechanical
op	operating
out	output
P	pump
rt	round-trip
RW	river water
spec	specific
ST	storage
T	turbine
th	thermal
tot	total
WG	water–glycol mixture

ACKNOWLEDGEMENTS

Open Access funding enabled and organized by Projekt DEAL.

ORCID

Josefine Koksharov http://orcid.org/0000-0001-9290-9817

Frank Dammel http://orcid.org/0000-0003-4021-8031

REFERENCES

1. Zhao Y, Song J, Liu M, et al. Thermo-economic assessments of pumped-thermal electricity storage systems employing sensible heat storage materials. *Renewable Energy*. 2022;186:431-456. doi:10.1016/j.renene.2022.01.017
2. Astolfi M. Technical options for Organic Rankine Cycle systems. In: Macchi E, Astolfi M, eds. *Organic Rankine Cycle (ORC) Power Systems: Technologies and Applications*. Joe Hayton; 2017:67-89.

3. Mercangöz M, Hemrle J, Kaufmann L, Z'Graggen A, Ohler C. Electrothermal energy storage with transcritical CO_2 cycles. *Energy*. 2012;45(1):407-415. doi:10.1016/j.energy.2012.03.013
4. Morandin M, Maréchal F, Mercangöz M, Buchter F. Conceptual design of a thermo-electrical energy storage system based on heat integration of thermodynamic cycles—Part A: methodology and base case. *Energy*. 2012;45(1):375-385. doi:10.1016/j.energy.2012.03.031
5. Morandin M, Maréchal F, Mercangöz M, Buchter F. Conceptual design of a thermo-electrical energy storage system based on heat integration of thermodynamic cycles—Part B: alternative system configurations. *Energy*. 2012;45(1):386-396. doi:10.1016/j.energy.2012.03.033
6. Morandin M, Mercangöz M, Hemrle J, Maréchal F, Favrat D. Thermoeconomic design optimization of a thermo-electric energy storage system based on transcritical CO_2 cycles. *Energy*. 2013;58:571-587. doi:10.1016/j.energy.2013.05.038
7. Baik YJ, Heo J, Koo J, Kim M. The effect of storage temperature on the performance of a thermo-electric energy storage using a transcritical CO_2 cycle. *Energy*. 2014;75:204-215. doi:10.1016/j.energy.2014.07.048
8. Steinmann WD, Jockenhöfer H, Bauer D. Thermodynamic analysis of high-temperature Carnot battery concepts. *Energy Technol*. 2020;8(3):1900895. doi:10.1002/ente.201900895
9. Zhao Y, Song J, Sapin P, Zhao Y, Markides CN. *Thermo-economic Optimisation and Comparison of Pumped Thermal Electricity Storage (PTES) System based on Transcritical Rankine Cycles*; 2nd International Workshop on Carnot Batteries, 2020.
10. De Rose A, Buna M, Strazza C, et al. *Technology Readiness Level: Guidance Principles for Renewable Energy technologies*; 2017. https://www.gransking.fo/media/2900/trl-orka.pdf
11. Lecompte S, Ntavou E, Tchanche B, et al. Review of experimental research on supercritical and transcritical thermodynamic cycles designed for heat recovery application. *Appl Sci*. 2019;9(12):2571. doi:10.3390/app9122571
12. Hedbäck A. *Pressureless Accumulator for District Heating Systems*; 2014. Accessed January 20, 2022. https://patentimages.storage.googleapis.com/b9/9a/da/bcd3b8db9c2c66/EP2698584A1.pdf
13. ENERKO. *ENERKO plant einen der größten Fernwärmespeicher Deutschlands*. Accessed April 23, 2023. https://enerko.de/themenspecial/enerko-plant-einen-der-groessten-fernwaermespeicher-deutschlands/
14. Bilfinger Industrial Services. *2-Zonen-Speicher - Referenzen*; 2022. Accessed January 21, 2022. https://bis-austria.bilfinger.com/referenzen/energie-versorgung-hydro/fernwaermespeicher/2-zonen-speicher/
15. Maximini M. *Flexibilisierung der Strom- und Wärmeerzeugung durch Wärmespeicher*; 2019. Accessed January 20, 2022. https://enerko.de/wp-content/uploads/2019/11/191120-Flexibilisierung-der-Strom-und-Waermeerzeugung-durch-Waermespeicher-.pdf
16. Macchi E. Theoretical basis of the Organic Rankine Cycle. In: Macchi E, Astolfi M, eds. *Organic Rankine Cycle (ORC) Power Systems: Technologies and Applications*. Joe Hayton; 2017:3-24.
17. Fraughton C. *Electro-Thermal Energy Storage—General Presentation*; 2021. Accessed January 21, 2022. https://netl.doe.gov/sites/default/files/netl-file/21TMCES_Fraughton.pdf
18. Decorvet RC, Jacquemoud E. *Industrial Heat Pumps—MAN Energy Solutions*; 2021. Accessed January 21, 2022. https://www.man-es.com/process-industry/campaigns/industrial-heat-pumps-and-ems#download
19. STEAG Energy Services. *Anlagen universell planen und optimieren - Fact Sheet*. Accessed February 4, 2022. https://www.steag.com/uploads/pics/Factsheet_EBSILON_de_01.PDF
20. STEAG Energy Services. *EBSILON®Professional Online Hilfe: Optimierung*. Accessed February 3, 2022. https://help.ebsilon.com/DE/Optimierung.html
21. National Institute of Standards and Technology. *Reference Fluid Thermodynamic and Transport Properties Database (REFPROP)*. Accessed February 3, 2022. https://www.nist.gov/programs-projects/reference-fluid-thermodynamic-and-transport-properties-database-refprop
22. Bao J, Zhao L. A review of working fluid and expander selections for Organic Rankine Cycle. *Renewable Sustainable Energy Rev*. 2013;24:325-342. doi:10.1016/j.rser.2013.03.040
23. Hassan AH, O'Donoghue L, Sánchez-Canales V, Corberán JM, Payá J, Jockenhöfer H. Thermodynamic analysis of high-temperature pumped thermal energy storage systems: refrigerant selection, performance and limitations. *Energy Rep*. 2020;6:147-159. doi:10.1016/j.egyr.2020.05.010
24. Sauret E, Rowlands AS. Candidate radial-inflow turbines and high-density working fluids for geothermal power systems. *Energy*. 2011;36(7):4460-4467. doi:10.1016/j.energy.2011.03.076
25. The European Parliament and the Council of the European Union. *Regulation (EU) No 517/2014 on Fluorinated Greenhouse Gases and Repealing Regulation (EC) No 842/2006*; 2014. Accessed February 4, 2022. https://eur-lex.europa.eu/legal-content/EN/TXT/PDF/?uri=CELEX:32014R0517&from=EN
26. Averfalk H, Benakopoulus T, Best I, et al. *Low-Temperature District Heating Implementation Guidebook*. Fraunhofer-Gesellschaft; 2021.
27. Turton R, Bailie RC, Whiting WB, Shaeiwitz JA, Bhattacharyya D. *Analysis, Synthesis and Design of Chemical Processes*. 4th ed. Pearson Education; 2013.
28. Wagner W. *Wärmeaustauscher - Grundlagen, Aufbau und Funktion technischer Apparate*. Vogel Business Media; 2015.
29. Oh HK, Son CH. New correlation to predict the heat transfer coefficient in-tube cooling of supercritical CO_2 in horizontal macro-tubes. *Exp Therm Fluid Sci*. 2010;34(8):1230-1241. doi:10.1016/j.expthermflusci.2010.05.002
30. Yoon SH, Kim JH, Hwang YW, Kim MS, Min K, Kim Y. Heat transfer and pressure drop characteristics during the in-tube cooling process of carbon dioxide in the supercritical region. *Int J Refrig*. 2003;26(8):857-864. doi:10.1016/S0140-7007(03)00096-3
31. Wang K, Xu X, Wu Y, Liu C, Dang C. Numerical investigation on heat transfer of supercritical CO_2 in heated helically coiled tubes. *J Supercrit Fluids*. 2015;99:112-120. doi:10.1016/j.supflu.2015.02.001
32. Kondou C, Hrnjak P. Condensation from superheated vapor flow of R744 and R410A at subcritical pressures in a horizontal smooth tube. *Int J Heat Mass Transfer*. 2012;55(11-12):2779-2791.

33. Selvam C, Balaji T, Mohan Lal D, Harish S. Convective heat transfer coefficient and pressure drop of water–ethylene glycol mixture with graphene nanoplatelets. *Exp Therm Fluid Sci*. 2017;80:67-76. doi:10.1016/j.expthermflusci.2016.08.013
34. Towler G, Sinnott R. *Chemical Engineering Design—Principles, Practice and Economics of Plant and Process Design*. Butterworth-Heinemann; 2013.
35. Roetzel W, Spang B. Typische Werte von Wärmedurchgangskoeffizienten. In: VDI e.V. ed. *VDI-Wärmeatlas*. Springer-Verlag; 2013:85-89.
36. Balli O, Aras H, Hepbasli A. Exergoeconomic analysis of a combined heat and power (CHP) system. *Int J Energy Res*. 2008;32:273-289.
37. Sanaye S, Shirazi A. Thermo-economic optimization of an ice thermal energy storage system for air-conditioning applications. *Energy Build*. 2013;60:100-109. doi:10.1016/j.enbuild.2012.12.040
38. Jenkins S. *2019 Chemical Engineering Plant Cost Index Annual Average*; 2020.Chemical Engineering. Accessed February 3, 2022. https://www.chemengonline.com/2019-chemical-engineering-plant-cost-index-annual-average/
39. European Commission. *Exchange rate (InforEuro)*. Accessed February 3, 2022. https://ec.europa.eu/info/funding-tenders/procedures-guidelines-tenders/information-contractors-and-beneficiaries/exchange-rate-inforeuro_en
40. Kost C, Shammugam S, Fluri V, Peper D, Memar AD, Schlegl T. *Stromgestehungskosten Erneuerbare Energien (Juni 2021)*; Studie, Fraunhofer–Institut für Solare Energiesysteme ISE. 2021.
41. Schmidt O, Melchior S, Hawkes A, Staffell I. Projecting the future levelized cost of electricity storage technologies. *Joule*. 2019;3(1):81-100. doi:10.1016/j.joule.2018.12.008
42. Steinmann W-D, Bauer D, Jockenhöfer H, Johnson M. Pumped thermal energy storage (PTES) as smart sector-coupling technology for heat and electricity. *Energy*. 2019;183:185-190. doi:10.1016/j.energy.2019.06.058
43. Krüger M, Schwarzenbart M, Zunft S. Verfahrensentwicklung für dezentrale adiabate Druckluftspeicherkraftwerke (Mini-CAES). In: *Thermodynamik-Kolloquium 2014*; 2014.
44. Amigun B, von Blottnitz H. Capital cost prediction for biogas installations in Africa: Lang factor approach. *Environ Prog Sustainable Energy*. 2009;28(1):134-142.
45. Bejan A, Tsatsaronis G, Moran M. *Thermal Design and Optimization*. Wiley-Interscience; 1996.
46. Dietrich A. *Assessment of Pumped Heat Electricity Storage Systems through Exergoeconomic Analyses*. Ph.D. Thesis Technische Universität Darmstadt; 2017.
47. ENTSO-E. *Transparency Platform*. Accessed May 10, 2023. https://transparency.entsoe.eu/
48. KfW. *KfW-Programm Erneuerbare Energien Standard*; 2022. Accessed February 4, 2022. https://bit.ly/3pwuZnM
49. KfW. *Konditionenübersicht für Endkreditnehmer*; 2022. Accessed February 4, 2022. https://www.kfw-formularsammlung.de/KonditionenanzeigerINet/KonditionenAnzeiger
50. Phillips PCB. Econometric analysis of Fisher's equation. *Am J Econ Sociol*. 2005;64(1):125-168.
51. Schlosser F, Jesper M, Vogelsang J, Walmsley TG, Arpagaus C, Hesselbach J. Large-scale heat pumps: applications, performance, economic feasibility and industrial integration. *Renewable Sustainable Energy Rev*. 2020;133:110219.
52. Decorvet RC. *MAN ETES (Electro Thermal Energy Storage)—With Industrial Heat Pump Technology Decarbonising Heat & Cold Supply and Energy Storage (Webinar)*; Man Energy Solutions, 2021. Accessed February 9, 2022. https://register.gotowebinar.com/register/3248652657847829006?source=website&action=registerwebinar
53. DIN Forsyning. *Seawater Replaces Coal*. Accessed February 4, 2022. https://fremtidensfjernvarme.dk/da-dk/green-and-eco-friendly-domestic-heating/seawater-replaces-coal
54. MAN Energy Solutions. *Pioneering Order for MAN ES*. Accessed February 4, 2022. https://people.man-es.com/strategy/pioneering-order-for-man-es
55. Baltimore Aircoil Company. *TSU-M*. Accessed February 4, 2022. https://www.baltimoreaircoil.eu/en/products/TSU-M
56. BEKA. *Ice Thermal Storage Technology from the Container*. Accessed February 4, 2022. https://www.beka-klima.de/en/ice-energy-storage/
57. FAFCO. *ICEBAT UW Internal Melt Ice Storage*. Accessed February 4, 2022. https://www.fafco.fr/en/icebat-uw-internal-melting-ice-storage-eng/
58. García-Pabón JJ, Méndez-Méndez D, Belman-Flores JM, Barroso-Maldonado JM, Khosravi A. A review of recent research on the use of R1234yf as an environmentally friendly fluid in the Organic Rankine Cycle. *Sustainability*. 2021;13(5864):5864. doi:10.3390/su13115864
59. Echogen Power Systems. *EPS100 Heat Recovery Solution*. Accessed February 4, 2022. https://www.echogen.com/our-solution/product-series/eps100/
60. Dincer I, Erdemir D. Heat storage methods. In: Rhodes R, ed. *Heat Storage Systems for Buildings*. Elsevier; 2021:37-90. doi:10.1016/b978-0-12-823572-0.00010-2
61. Thess A. Thermodynamic efficiency of pumped heat electricity storage. *Phys Rev Lett*. 2013;111:110602. doi:10.1103/PhysRevLett.111.110602
62. Chen J, Guo J. Comment on 'Thermodynamic efficiency of pumped heat electricity storage'. *Phys Rev Lett*. 2016;116:158901. doi:10.1103/PhysRevLett.116.158901
63. Roskosch D, Venzik V, Atakan B. Potential analysis of pumped heat electricity storages regarding thermodynamic efficiency. *Renew Energy*. 2020;147:2865-2873. doi:10.1016/j.renene.2018.09.023
64. Vecchi A, Knobloch K, Liang T, et al. Carnot battery development: a review on system performance, applications and commercial state-of-the-art. *J Energy Storage*. 2022;55:105782. doi:10.1016/j.est.2022.105782
65. Benato A. Performance and cost evaluation of an innovative pumped thermal electricity storage power system. *Energy*. 2017;138:419-436. doi:10.1016/j.energy.2017.07.066

How to cite this article: Bodner J, Koksharov J, Dammel F, Stephan P. Analysis of low-temperature pumped thermal energy storage systems based on a transcritical CO_2 charging process. *Energy Sci Eng*. 2023;11:3289-3306. doi:10.1002/ese3.1505